

RankMap: A Platform-Aware Framework for Distributed Learning from Dense Datasets

Azalia Mirhoseini¹, Eva. L. Dyer², Ebrahim. M. Songhori³, Richard Baraniuk⁴, and Farinaz Koushanfar¹

Dept. of Electrical and Computer Engineering, Rice University, Houston, TX^{1,3,4,5}

Dept. of Physical Medicine and Rehabilitation, Northwestern University; Rehabilitation Institute of Chicago²

azalia¹, ebrahim³, richb⁴, farinaz⁵@rice.edu

edyer²@ric.org

ABSTRACT

This paper introduces RankMap, a platform-aware end-to-end framework for efficient execution of a broad class of iterative learning algorithms for massive and dense datasets. In contrast to the existing dense (iterative) data analysis methods that are oblivious to the platform, for the first time, we introduce novel scalable data transformation and mapping algorithms that enable optimizing for the underlying computing platforms' cost/constraints. The cost is defined by the number of arithmetic and (within-platform) message passing operations incurred by the variable updates in each iteration, while the constraints are set by the available memory resources. RankMap transformation scalably factorizes data into an ensemble of lower dimensional subspaces, while its mapping schedules the flow of iterative computation on the transformed data onto the pertinent computing machine. We show a trade-off between the desired level of accuracy for the learning algorithm and the RankMap's achieved efficiency. RankMap provides two APIs, one matrix-based and one graph-based, which facilitate automated adoption of the framework for performing several contemporary iterative learning applications optimized to the platform. To demonstrate the utility of RankMap, we solve sparse recovery and power iteration problems on various real-world datasets with up to 1.8 billion non-zeros. Our evaluations are performed on Amazon EC2 and IBM iDataPlex platforms using up to 244 cores. The results demonstrate up to 2 orders of magnitude improvements in memory usage, execution speed, and bandwidth compared with the best reported prior work.

1. INTRODUCTION

Many modern learning algorithms are based on exploring the underlying patterns, correlations, and dependencies present across the signals in the dataset. Some prominent

examples of such algorithms and their applications are linear or penalized regression, power iterations, belief propagation, and expectation maximization [1, 2]. In all of these settings, solving the underlying objective function requires iterative updates of parameters of interest until convergence is achieved. Such iterative updates often require matrix multiplications that involve the data dependency or Gram matrix. In scenarios where data is too large to fit on a single computing node and must be distributed, iterative dependency-based updates become highly challenging as they incur large computation and communication costs.

A number of distributed abstractions that target iterative learning algorithms have been developed, e.g., Pregel [3], and GraphLab [4]. These abstractions adopt a graph-parallel model which consists of a *sparse graph* and a kernel function that runs in parallel on each vertex [5]. Performance gains are achieved due to the communication-minimizing partitioning of the graph and effective control of data movement.

While graph-parallelism has been shown to accelerate machine learning and signal processing tasks for sparse graphs, this approach cannot be readily applied when the data exhibit a *non-sparse dependency matrix*. The storage of such data in the graph format becomes very inefficient as it requires storing large number of edges (corresponding to dense dependencies) for each vertex. In addition, finding efficient graph cuts and partitions is infeasible when dense dependencies exist. Data with dense dependencies appear in a wide range of important fields such as computer vision, medical image processing, the boundary element methods and their applications, and N-body problems [6, 7]. Thus, finding efficient solutions for running iterative learning algorithms on densely dependent data is of paramount importance.

In this paper, we introduce RankMap, a novel distributed framework for efficient execution of a broad class of iterative learning algorithms on datasets with dense dependencies. Our key observation is that, despite the apparent high dimensionality of data, in many settings dense datasets are low rank or lie on a union of much lower dimensional subspaces. We exploit this property to reduce the overhead of data dependencies, a factor which has rendered the currently available graph-parallel abstractions impractical for processing dense datasets. RankMap provides a set of interfaces and transformations that enable efficient data-aware content analysis, as well as coordinated mapping and optimization of the underlying hardware components. Our

overarching goal is to reduce the following critical metrics in high performance distributed computing systems: execution runtime, memory usage, and communication overhead.

To accelerate matrix vector multiplications required to compute an iterative update, we decompose dense but structured data and rewrite it as a product of two matrices with far fewer non-zeros than the original data. The shrunk decomposed data is then used in subsequent iterative learning algorithms. We introduce a host of automated methods for partitioning the decomposed factors and ordering the computation flow in a distributed setting. The partitioning algorithm is efficient (within a bound from the optimum) and has a constant runtime. We introduce two different representations and accompanying computational models (a matrix-based and a vertex-centric model) to compute an update. We show that depending on the data domain and the sparsity of the decomposed components, there are different regimes where each of these two models deliver highest efficiency.

We provide APIs for both matrix-based and vertex-centric iterative update models on the transformed data. Our matrix-based API uses the general Message Passing Interface (MPI). Our vertex-centric API is written based on the GraphLab programming model. We develop an efficient mapping of the iterative computations on the sparsified decomposed data within the constraints of the GraphLab distributed framework. Both APIs are written in C++. We evaluate RankMap on the Amazon Elastic Cloud (EC2) computing service and the IBM iDataPlex computer cluster. Our experiments utilize up to 244 cores on 12 large computing nodes. The RankMap APIs are open source and shall be freely available to download (hidden to observe anonymity). Our explicit contributions are as follows:

- We propose the RankMap framework, a suite of domain-specific transformations and distributed interfaces that enable executing a large set of popular knowledge extraction algorithms on big and dense data. Based upon learning the domain data, dependency structure, and the properties of the underlying hardware, RankMap provides an efficient resource-aware mapping of the computation onto the distributed setting.
- (Section 4) We introduce a novel scalable transformation which maps a dense and structured data onto two matrices which contain fewer number of non-zeros. The resulting decomposition can be used for improving the performance of several important iterative learning algorithms that exploit data dependencies. We provide a systematic way to tune the decomposition error to achieve a desired level of accuracy in the learning applications.
- (Section 5) We develop efficient distributed computational models to conduct iterative updates on the decomposed data. Highly effective partitioning methods for the decomposed data along with data-aware performance bounds are provided.
- (Section 6) We perform proof-of-concept evaluation on applications including eigenvalue decomposition, denoising, and classification that demonstrate up to 2 orders of magnitude improvement in runtime and memory footprint.
- (Section 7) We discuss the practicality of RankMap and domain-specific use-cases of each of the proposed

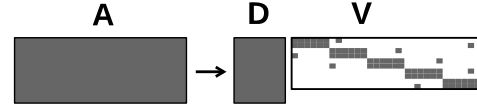


Figure 1: Schematic depiction of decomposing dense data dependencies into a large sparse component and a small dense one.

computational models.

2. RankMap FRAMEWORK

2.1 Overview and approach

In this paper, we introduce RankMap, a distributed data-aware framework that efficiently executes learning algorithms that rely on costly iterative updates on dense Gram matrices. The main idea underlying our approach is to leverage structure in large collections of data to decompose the Gram matrix such that the system costs (e.g, runtime, memory, and energy) associated with iterative learning algorithms are significantly reduced.

Let the data matrix $\mathbf{A} \in \mathbb{R}^{m \times n}$ denote a collection of n signals of m -dimensions, and $\mathbf{G} = \mathbf{A}^T \mathbf{A}$ denote the Gram matrix. Many learning algorithms iteratively update a solution vector, denoted by \mathbf{x} , according to an update function of the following form:

$$\mathbf{x}^{iter+1} = f(\mathbf{G}\mathbf{x}^{iter}), \quad (1)$$

where $f(\cdot)$ is a low-complexity function.

When \mathbf{G} is massive and dense, each distributed update becomes very expensive. Thus, RankMap creates an approximation to \mathbf{G} , denoted by $\hat{\mathbf{G}}$, to reduce the cost of an update. To be more specific, our aim is to decompose the data matrix \mathbf{A} into two components, i.e., $\hat{\mathbf{A}} = \mathbf{D}\mathbf{V}$, where $\mathbf{D} \in \mathbb{R}^{m \times l}$ contains a subset of columns from \mathbf{A} , $\mathbf{V} \in \mathbb{R}^{l \times n}$ is a sparse matrix, and $\text{rank}(\mathbf{A}) \leq l \ll n$ (Figure 1). After decomposing \mathbf{A} , we then efficiently partition the decomposed data and perform distributed updates using $\hat{\mathbf{G}} = (\mathbf{D}\mathbf{V})^T (\mathbf{D}\mathbf{V})$. Mapping the original dense data to a decomposed model directly reduces the memory usage, and the costly computational operations and communication incurred by the iterative updates.

When \mathbf{A} is exactly low rank (single low-dimensional subspaces) or lies on a small number of low-dimensional subspaces, the aforementioned decomposition is exact. However, we demonstrate that for many real-world datasets, we can achieve significant performance improvements in exchange for a small decomposition error. We discuss the connection between the decomposition error and the accuracy of a target learning method as well as strategies for tuning the decomposition to achieve a desired level of accuracy in the iterative learning algorithms.

Figure 2 shows an overview of our framework. RankMap consists of three main components: (i) A scalable data decomposition that shrinks the size of the domain content by leveraging the data’s structured properties, (ii) A data partitioning scheme along with an execution flow for performing iterative updates on the decomposed data that significantly reduces the distributed computing costs, (iii) a

$\mathbb{R}^{n \times k}$ are the truncated singular vectors (first k columns of \mathbf{U} and \mathbf{V}) and $\Sigma_k \in \mathbb{R}^{k \times k}$ contains the first k singular values of \mathbf{A} along its diagonal. The rank equals the number of non-zero singular values or $\text{rank}(\mathbf{A})$. The truncated SVD also provides the solution to principal components analysis (PCA), which seeks to find a k -dimensional subspace that best approximates \mathbf{A} in the least-squares sense.

The complexity of computing the SVD directly is m^2n . Thus, for large datasets, the power method is used to find the eigenvectors of $\mathbf{A}^T \mathbf{A}$ and $\mathbf{A} \mathbf{A}^T$, which correspond to the right and left singular vectors respectively.

3.1.2 Sparse factorization

The SVD provides a closed-form solution for finding the best rank- k approximation to a matrix. However, in many settings, enforcing sparse structure, either in the left or right singular vectors can provide a more faithful and compact decomposition of the data. Two widely used sparse factorization methods include sparse PCA (SPCA) [14] and dictionary learning (DL) [15]. However, these approaches are often not applied to large datasets since computing an update of both the left and right factor matrices, at each iteration is costly. To solve SPCA on big datasets, a generalized power method can be employed [16]. The basic idea behind using the power method to find sparse principal components is to simply threshold the output of each power iteration to ensure the resulting eigenvectors are sparse. Unfortunately, the convergence of this method is much slower than standard power iterations.

3.1.3 Column subset selection (CSS)-based matrix factorization

In contrast to methods such as PCA and its sparse variants, an alternative strategy for low rank matrix factorization is to form a decomposition based upon columns (or row) from the data. CSS-based solutions form an approximate matrix decomposition in which one factorized component is a subset of the columns of the data itself [17]. CSS-based approaches have been used to provide a scalable and efficient strategy for finding approximate solutions to least-squares regression [18], Gramian matrix decomposition [17], and also in spectral clustering [19]. In all of the aforementioned settings, CSS is employed to select a few columns from \mathbf{A} and a low rank decomposition is obtained by projecting the data onto the subspace spanned by this set of columns. Our proposed data decomposition approach leverages a CSS-based to form the left factor matrix \mathbf{D} .

3.2 Generic distributed abstractions

A number of successful distributed abstractions for processing large datasets on clusters have been proposed. Examples include MapReduce [20], Apache Spark [21], and SystemML [22]. However these models become less efficient for applications when direct data-parallelism does not exist. Several new distributed abstractions have been proposed that model data dependency in a graph format, most notably Pregel [3] and GraphLab [4]. They use a vertex-centric computation model, in which the user-defined programs are executed on each vertex in parallel. However, graph-based abstractions are suited for sparse datasets as efficient data partitioning is not possible when data is densely connected. Furthermore, such tools mostly rely on the communication between the vertices for computation. When the data is

densely connected, the resulting communication congestion makes the computation dramatically slow. Because of this, most of these tools are designed based on the assumption that the input data is sparse [5, 3, 21].

4. COLUMN SELECTION-BASED SPARSE DECOMPOSITION (CSSD)

In this section, we present a scalable method for matrix decomposition (the Decomposition phase in Figure 2) which we call Subsampled Sparse Matrix Decomposition (CSSD).

4.1 Overview of CSSD method

The main idea behind CSSD is to: (i) select a subset of columns from a matrix and (ii) use this subset of columns as a basis from which we form sparse representations of the remaining columns in the dataset. To be precise, if we consider a factorization of $\mathbf{A} = \mathbf{D}\mathbf{V}$, the matrix \mathbf{D} is formed by subsampling and normalizing columns of \mathbf{A} and each column of \mathbf{V} is computed by finding the sparse approximation of the corresponding column of \mathbf{A} with respect to \mathbf{D} . This sparse approximation problem can be solved by an efficient greedy routine called *orthogonal matching pursuit* (OMP) [23]. We provide pseudocode for CSSD in Alg. 1.

4.1.1 Step 1. Sequential column selection

In order to ensure that the total approximation error in our factorization is sufficiently small, we must ensure that the columns selected from \mathbf{A} to form \mathbf{D} well approximate the range of the original matrix. Thus, a number of column sampling approaches employ a sequential method to adaptively select columns that are not well approximated by the current set of columns [24].

Adaptive column selection methods consist of two main steps. First, we compute the projection error $\mathbf{E} = \mathbf{A} - \mathbf{A}_S \mathbf{A}_S^+$ based upon the current set of selected columns given by \mathbf{A}_S^1 . Second, we select a new batch of columns according to the following probability distribution:

$$p(i) \propto \frac{\|\mathbf{A}_S \mathbf{A}_S^+ \mathbf{a}_i - \mathbf{a}_i\|_2}{\|\mathbf{a}_i\|_2}, \quad (5)$$

where $p(i)$ equals the probability of selecting the i^{th} column from \mathbf{A} , given by \mathbf{a}_i . This subsampling approach can be used by either specifying the maximum number of columns to select and/or specifying the maximum amount of error in each column of \mathbf{A} .

4.1.2 Step 2. Sparse approximation

After selecting a subset of l columns $\mathbf{A}_S \in \mathbb{R}^{m \times l}$, we normalize each column to produce a matrix with unit norm columns \mathbf{D} . Now, to form the sparse matrix \mathbf{V} , we find a sparse representation of the remaining columns in \mathbf{A} (i.e., \mathbf{A}_{-S}) in terms of the normalized dictionary \mathbf{D} . The problem is formally written as follows:

$$\forall \mathbf{a} \in \mathbf{A}_{-S} \text{ solve: } \min_{\mathbf{v}} \|\mathbf{v}\|_0 \text{ s.t. } \frac{\|\mathbf{a} - \mathbf{D}\mathbf{v}\|_2}{\|\mathbf{a}\|_2} \leq \delta_D. \quad (6)$$

We employ a matching pursuit-based solver called Batch OMP [25] to solve Equation 6. The solver allows us to enforce sparsity either by fixing the number of non-zeros in

¹The pseudo-inverse is calculated as: $\mathbf{A}^+ = (\mathbf{A}^T \mathbf{A})^{-1} \mathbf{A}^T$.

Algorithm 1 : CSSD

Input: Matrix $\mathbf{A} \in \mathbb{R}^{m \times n}$, error tolerance δ_D , number of columns to select at each iteration l_s , and the maximum number of columns to select l .

Output: A sparse matrix $\mathbf{V} \in \mathbb{R}^{l \times n}$ and a dense matrix $\mathbf{D} \in \mathbb{R}^{m \times l}$ such that for each column \mathbf{a} of \mathbf{A} , $\|\mathbf{a} - \mathbf{D}\mathbf{v}\|_2 \leq \delta_D$.

Initialize: Initialize \mathbf{D} by adding and normalizing l_s columns from \mathbf{A} with uniform random sampling.

Step 1: Sequential column selection

while $ncols(\mathbf{D}) < L$ **do**

- I. Update \mathbf{D} by selecting and normalizing l_s columns from \mathbf{A} according to the distribution in Equation 5.
- II. If the ℓ_2 -norm of each column of $\mathbf{E} = \mathbf{A} - \mathbf{D}\mathbf{D}^+\mathbf{A}$ is less than δ_D , return \mathbf{D} and proceed to Step 2 to compute \mathbf{V} .

end while

Step 2. Sparse approximation

- I. Compute \mathbf{V} by applying Batch OMP to solve Equation 6 with error tolerance δ_D .
-

each column of \mathbf{V} (i.e., $\|\mathbf{v}\|_0$) or by fixing the total amount of approximation error for each column (i.e., δ_D).

4.2 Complexity analysis

The complexity of sequential column selection (Step 1) is $\mathcal{O}(l^2m + lmn)$. The complexity terms in turn correspond to computing \mathbf{D}^+ and $\mathbf{D}\mathbf{D}^+\mathbf{A}$. For each column \mathbf{a} of \mathbf{A} , $\mathbf{D}\mathbf{D}^+\mathbf{a}$ can be computed independently. The complexity of sparse approximation (Step 2), using the Batch OMP method [25], is $\mathcal{O}(lmn + k^2ln)$, where $k < l$ is the average number of non-zeros per column of \mathbf{V} . Similarly, for each column \mathbf{a} of \mathbf{A} , Batch OMP is applied independently. Let n_c be the number of parallel processing nodes. By storing \mathbf{D} (which is a small $m \times l$ matrix) and a uniform fraction of columns of \mathbf{A} in each node (i.e., $\frac{n}{n_c}$ columns), the overall complexity of Algorithm 1 in a distributed setting can be written as $\mathcal{O}(\frac{n}{n_c}(lm + k^2l) + l^2m)$.

Note that the scalability of CSSD is a crucial property which makes our framework applicable to very large datasets (large n) in distributed settings.

4.3 Computational benefits of CSSD

CSSD provides computational benefits when the size of the decomposition is small (i.e., l is small relative to m) and/or when matrix \mathbf{V} is sparse. In general, predicting the amount of savings in computation is a function of (i) the structure of the data and (ii) the amount of accuracy required from the learning algorithm. We now discuss some key factors that impact the decomposition results.

Impact of data structure. Predicting the size and sparsity of the decomposition provided by CSSD for an arbitrary dataset is challenging; however, when the data lies on a single subspace (i.e., exhibits low rank structure) or lies on multiple low-dimensional subspaces, CSSD provides a more compact representation of the data. For example, for when data is exactly low rank and its rank is $r < m$, we must select r linearly independent columns from \mathbf{A} to form an exact decomposition (zero error), i.e., $l = r$. When the data

is approximately low rank, there exists a large body of work that characterizes the performance of the sequential column selection method (Step 1) used to form \mathbf{D} . In particular, the selection strategy in Step 2 of Algorithm 1 provides exponential decrease in the factorization error with each batch of columns that we select from \mathbf{A} [24]. More specifically, assume that at each iteration, we select $l_s > \frac{r}{\epsilon}$ samples from the columns of \mathbf{A} and let $l = tl_s$ denote the set of columns selected after t iterations. Let \mathbf{A}_r denote the best rank r approximation to \mathbf{A} and let $\tilde{\mathbf{A}} = \mathbf{A}_S \mathbf{A}_S^+ \mathbf{A}$ denote the approximation of \mathbf{A} based upon the l selected columns. Then according to [24], the difference between the expected value of the approximation error, i.e., $\|\mathbf{A} - \tilde{\mathbf{A}}\|_F^2$ and that of the best rank r approximation $\|\mathbf{A} - \mathbf{A}_r\|_F^2$ decreases exponentially with rate ϵ^t .

Another low-dimensional signal model that has recently gained traction captures a collection of data with multiple low-dimensional subspaces (union of low-dimensional subspaces). For example, images of objects under different illumination conditions [26], motion trajectories of point-correspondences [27], to structured sparse and block-sparse signals [28] are all well-approximated by a union of low-dimensional subspaces. When \mathbf{A} lies on a union of subspaces, this effectively bounds the sparsity level of each column of \mathbf{V} [29]. This insight is based upon the fact that when we form a representation of a column of \mathbf{A} with respect to other columns in the same dataset (as in CSSD), the sparsity level of each column is bounded by the dimension of the subspace the signal lies on. For instance, if \mathbf{A} lives on a union of multiple r -dimensional subspaces of \mathbb{R}^n and we select at least r linearly independent columns from each subspace, then no more than r non-zeros must be used to represent a signal. In other words the number of non-zeros per column of \mathbf{V} is no more than r .

Impact of increasing the decomposition error δ_D . The decomposition error of CSSD is controlled by the parameter δ_D in Algorithm 1. In the case where we set $\delta_D = 0$, then we are guaranteed an exact decomposition of the data. Exact decomposition occurs when m linearly independent columns are selected from \mathbf{A} ; in this case, the selected columns in \mathbf{A}_S will span the ambient dimension of the data \mathbb{R}^m and thus $\|\mathbf{A} - \mathbf{A}_S \mathbf{A}_S^+ \mathbf{A}\| = 0$, i.e., exact decomposition occurs.

While CSSD can produce an exact and compact decomposition when the data is exactly low rank (or lies on a union of subspaces), in practice, datasets are approximately low rank. In this case, we can introduce a small amount of error into the decomposition by setting $\delta_D > 0$. By introducing some error into the decomposition, we observe that both the number of selected columns in Step 1 of Algorithm 1 and the sparsity level of \mathbf{V} can be reduced further. In Figure 7 we show how increasing the decomposition error produces a more compact result.

4.4 Impact of decomposition error on learning accuracy

In the previous section, we discussed the computational benefits associated with introducing some approximation error into a CSSD decomposition. Naturally, as we increase the decomposition error (controlled by δ_D) the accuracy of our learning algorithm (learning error) also increases. Thus, the key question is how much decomposition error we can

afford to achieve a certain degree of accuracy in learning. The answer to this question heavily depends on the specific learning algorithm and the application of interest.

Previous theoretical work have established a connection between the total error in a factorization of a kernel (or Gram) matrix (δ_D) and the accuracy of certain popular learning algorithms, including: kernel ridge regression and kernel SVM [30]. While for some learning algorithms, our framework can exploit the existing work in the literature to relate δ_D and the learning error which we denote by δ_L , the aim of this section is to propose a generic approach for tuning the factorization error to achieve a specified learning accuracy. In the following we introduce an approach for iteratively remapping of the data to find a compact decomposition that satisfies a pre-specified amount of learning error.

4.5 Error tuning

Given an already established relationship between the decomposition error and a specific algorithm, a practitioner who uses our framework can easily specify the error parameter δ_D for CSSD to achieve a particular learning accuracy. Alternatively, if a practitioner specifies a target accuracy for a learning algorithm, the decomposition error δ_D can be tuned in order to achieve a particular learning error δ_L .

Our strategy for guaranteeing that we have small δ_L , is to solve CSSD for a particular δ_D , map the resulting decomposition via the methods described in Section 5, and then approximate the accuracy of a learning algorithm δ_L . Once the decomposition error δ_D is small enough then we can ensure that δ_L is small as well. Depending on the underlying computing resources available, RankMap can be applied for multiple values of δ_D in parallel and the largest value of δ_D (most compact representation) that achieves a particular value of δ_L is selected.

When computing resources are constrained and thus running the algorithm for multiple values of δ_D in parallel is not possible, we use the bisection method. In essence, the idea is to: (i) set the factorization error to predefined maximum value δ_D^{max} (0.4 in our experiments) and evaluate δ_L , (ii) if δ_L is below a target value then we stop, otherwise we decrease δ_D by half. By exponentially decreasing δ_D , we are also guaranteed to decrease δ_L exponentially, provided that there is a polynomial relationship between the two variables. We observe a polynomial relationship holds both in theory [30] and in practice. In Section 6, we supply empirical results which demonstrate the connection between the decomposition error and learning accuracy for numerous datasets and algorithms of interest (see Figures 6b and 7b).

5. DISTRIBUTED EXECUTION AND DATA PARTITIONING

In this section, we introduce our approach for applying iterative updates on the decomposed data (the execution phase in Figure 2). We describe an execution flow for dependency-matrix based updates, i.e., $\mathbf{G}\mathbf{x} = \mathbf{V}^T(\mathbf{D}^T\mathbf{D})\mathbf{V}\mathbf{x}$, and introduce an efficient method for partitioning the decomposed data in a distributed setting. We also provide performance bounds on memory usage, number of flop operations, and number of communicated bytes across the computing nodes.

5.1 Computation flow

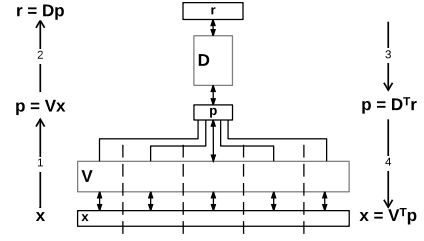


Figure 3: Distributed design of matrix-based model.

We propose two computational models for the distributed implementation of an update in Equation 1. Recall that at each iteration, we must compute $\mathbf{z} = \mathbf{G}\mathbf{x} = \mathbf{V}^T(\mathbf{D}^T\mathbf{D})\mathbf{V}\mathbf{x}$. We break this computation into four steps: (i) $\mathbf{p} = \mathbf{V}\mathbf{x}$ (ii) $\mathbf{r} = \mathbf{D}\mathbf{p}$, (iii) $\mathbf{p} = \mathbf{D}^T\mathbf{r}$, and (iv) $\mathbf{z} = \mathbf{V}^T\mathbf{p}$. The output vector \mathbf{z} is used to produce an update of $\mathbf{x}^{iter+1} = f(\mathbf{z} + \mathbf{b})$, where \mathbf{b} is a constant and $f(\cdot)$ is a low-complexity function such as a soft-thresholding operator (sparse approximation) or normalization (power method). To carry out the computation described above, we propose and implement a matrix-based and vertex-based model to apply the iterative updates on the decomposed factors. We now describe our implementation of both models.

5.2 Matrix-based model

Figure 3 shows the schematic of our proposed matrix-based model. In this model, data is stored as arrays. Sparse matrix \mathbf{V} is stored and operated upon using the Compressed Sparse Column (CSC) format. Matrices \mathbf{D} and vector \mathbf{x} are stored using regular dense arrays. By doing so, we exploit sparsity in \mathbf{V} . We use C++ Eigen Library for array manipulation and MPI for distributed computing.

5.2.1 Distributed partitioning

We partition columns of \mathbf{V} uniformly across the computing nodes to achieve a balanced partitioning. Let us assume that there are n_c computing nodes. Thus, $\frac{n}{n_c}$ number of columns are assigned to each node. Vector \mathbf{x} is also divided into chunks of size $\frac{n}{n_c} \times 1$. Each chunk is then allocated to the node that hosts the corresponding columns of \mathbf{V} .

Matrix-vector multiplications $\mathbf{V}\mathbf{x}$ are performed locally on the columns of \mathbf{V} and portion of \mathbf{x} that reside on the same computing node. The resulting $l \times 1$ vectors are then sent to a central node to create $\mathbf{p} = \mathbf{V}\mathbf{x}$. Next, $\mathbf{D}^T(\mathbf{D}\mathbf{p})$ is computed locally in the central node. The resulting $l \times 1$ vector is then *broadcasted* back to all the computing nodes where it is multiplied by the local \mathbf{V}^T to update the vector \mathbf{x} .

5.2.2 Performance bounds

We now provide bounds on the memory usage, computation, and communication required by our proposed matrix-based model. Let $nnz(\cdot)$ denote the number of non-zeros of its input and n_c denote the number of computing nodes. Recall that \mathbf{D} is a $m \times l$ matrix and \mathbf{V} is a $l \times n$ matrix.

- **Memory usage**
non-zeros $\propto (nnz(\mathbf{V}) + lm) + n + m$.
- **Computation** (per iteration)
additions $\propto 2(nnz(\mathbf{V}) + lm + ln_c)$
multiplications $\propto 2(nnz(\mathbf{V}) + lm)$

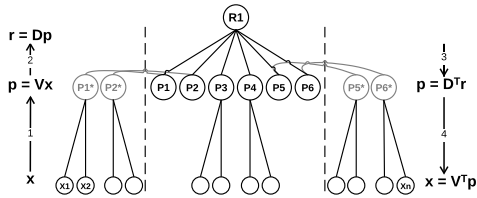


Figure 4: Distributed design of graph-based model.

- **Communication**

$$\# \text{edges} \propto 2ln_c.$$

Since matrix \mathbf{V} is stored in a CSC format, only the non-zero values are stored and operated on. Matrix \mathbf{D} is stored in a regular dense matrix format. The communication corresponds to sending and receiving the $l \times 1$ vectors from each computing node to the central node. As can be seen, for smaller l and sparser \mathbf{V} , both memory footprint and the number of arithmetics is reduced. The number of edges, which correspond to the number of broadcasted and reduced values, directly corresponds to l and the number of computing nodes n_c .

5.3 Graph-based model

Figure 4 shows an schematic of the graph model. The decomposed data graph denoted by $\mathcal{G}_A(S_X, S_P, S_R)$ is a 3-layer graph with vertex sets $S_X = \{X_i\}_{i=1}^n$ in the bottom layer, $S_P = \{P_i\}_{i=1}^l$ in the middle layer, and $S_R = \{R_1\}$ in the top layer. Each non-zero element in \mathbf{V} , e.g., V_{ij} , is represented by an edge which connects X_i to P_j . Each column of \mathbf{D} , e.g., D_i , is represented by an edge which connects P_i to R_1 . Value of vertices in S_X correspond to the elements of \mathbf{x} .

We use GraphLab Distributed API [4] to implement this model. While GraphLab is a highly optimized distributed engine for Graph-based computation on iterative data, we perform extensive customizations in order to adapt GraphLab to our factorized setting. We also force GraphLab to use our developed graph partitioning method as opposed to its automated partitioning schemes. Our proposed partitioning is customized to the factorized data and significantly improves the performance.

5.3.1 Distributed partitioning

In the graph-based model, we partition $\mathcal{G}_A(S_X, S_P, S_R)$ with the aim of balancing the number of components assigned to each node and also minimizing the inter-node communications characterized by the edges. Since the edge distribution of \mathcal{G}_A is highly non-uniform ($l \ll n$), a vertex partitioning inevitably results in many undesirable edge-cuts across the computing nodes. Instead, we apply a vertex-cut method in which the goal is to partition graph edges evenly such that the number of vertices that are spanned across multiple partitions is minimized. As a results of edge partitioning, in our implementation, vertices may reside onto two or more computing nodes. In this case we assign one of the copies to be the *master* vertex and the others to be the *replica* vertices (these definitions are borrowed from GraphLab [5]). The replicas directly cause (expensive) inter-node communication costs.

Figure 4 shows the graph-based distributed design. Our detailed edge partitioning method is as follows. (i) Dis-

tribute master of vertices $X_i \in S_X$ uniformly onto the available computing nodes such that vertex chunks of size $\frac{n}{n_c}$ are assigned to each node. (ii) Add the edges between vertices $X_i \in S_X$ and $P_j \in S_P$ to the node in which the corresponding master of X_i resides. (iii) Add master of vertices $P_i \in S_P$ and $R_1 \in S_R$ to a *central node*. and (iv) Add the edges between the vertices $P_i \in S_P$ and $R_1 \in S_R$ to the central node.

The proposed edge partitioning algorithm is highly efficient in that it does not induce any replicas for vertices in S_X and S_R . However from Step (ii) of the algorithm, replicas of vertices in S_P may exist in computing nodes other than the central node. At the beginning of an iteration, master vertices in S_P and their replicas perform vertex updates with respect to S_X . The replicas send the updated values to their own master vertices in the central node. The master vertices in S_P *reduce* the received values ($\mathbf{p} = \mathbf{V}\mathbf{x}$). Then master vertex R_1 performs a vertex update ($\mathbf{r} = \mathbf{D}\mathbf{p} - \mathbf{y}$). Next master vertices in S_P complete vertex updates with respect to S_R and *broadcast* the results to their own replicas ($\mathbf{p} = \mathbf{D}^T \mathbf{r}$). Finally master vertices in S_X update themselves ($\mathbf{x} = \mathbf{V}^T \mathbf{p}$). We integrate and implement the proposed customized partitioning and distributed computation flow with the distributed GraphLab API [5].

5.3.2 Performance bounds

We now provide bounds on the memory usage, computation, and communication required by our proposed graph-based model.

- **Memory usage**

$$\# \text{ edges} \propto nnz(\mathbf{V}) + l.$$

$$\# \text{ vertices} \propto n + \sum_{1 \leq i \leq l} rep(P_i).$$

- **Computation** (per iteration)

$$\# \text{ additions} \propto 2(nnz(\mathbf{V}) + ml) + \sum_{1 \leq i \leq l} rep(P_i).$$

$$\# \text{ multiplications} \propto 2(nnz(\mathbf{V}) + ml).$$

- **Communication**

$$\# \text{ edge-cuts} \propto 2 \sum_{1 \leq i \leq l} rep(P_i).$$

Each of the computing nodes receive approximately $\frac{1}{n_c}(n + \sum_{1 \leq i \leq l} rep(P_i))$ vertices and $\frac{1}{n_c}nnz(\mathbf{V})$ edges. The central node has l additional edges between the master vertices in S_P and R_1 . The computation cost is induced by vertex update operations. The communication overhead is incurred by the message passing across master and replica vertices in S_P .

Bound on total replicas. From above discussions, it is clear that reducing number of replicas of S_P reduces the communication overhead. The following are the bounds on the total number of replicas: $l \leq \sum_{1 \leq i \leq l} rep(P_i) \leq ln_c$. The inequalities hold since each P_i is replicated at least once and at most n_c times (one replica per computing node). Both l and n_c are much smaller than the size of the graph. Thus, RankMap’s graph-based model readily provides efficient/balanced computation and reduced communication without using complicated and costly graph partitioning algorithms. The minimum communication is achieved when \mathbf{V} is block-diagonal.

6. EVALUATIONS

In this Section, we evaluate the performance of RankMap on a diverse set of real-world and synthetic datasets. The real datasets include Light Field data from [31], hyper spectral images from [32], a dictionary of video frames from [33],

and a collection of images of different faces under varying illumination conditions [34]. We study the scaling behavior of CSSD, the connection between decomposition error and learning accuracy, and timing and performance of our distributed matrix and graph-based models.

6.1 Evaluation setup

6.1.1 Datasets

We apply RankMap to two different light field datasets. The first dataset, which we refer to as Light Field (i), consists of 10k randomly selected atoms from a 5×5 light field array (collected from Chess Images). Each light field patch consists of 25×8 -patches which produces a dataset of size $1.6k \times 10k$ (128MB). The second dataset, which we refer to as Light Field (ii), consists of 100k randomly selected atoms from a 17×17 light field arrays (collected from all available light fields in the archive). Each light field patch consists of 289×8 -patches which produces a dataset of size $18496 \times 100k$ (14.7GB). The hyper spectral dataset (Salinas) is taken from a region of a remote sensing scene in Salinas, CA; each pixel in the scene contains information from 203 spectral bands and produces a dataset of size 203×54129 (87.9MB). The video dictionary dataset (VideoDict) contains patches of an image over multiple frames and produces a dataset of size 1764×100000 (168MB). The face image dataset (Faces) consists of 631 images of 10 different peoples faces under varying illumination conditions. Each image is 48×84 pixels, which produces a dataset of size 4032×631 . In addition to real-world datasets, we generate synthetic decomposed data for $n = 10M$, $m = 1k$ with varying l and sparsity levels in \mathbf{V} .

6.1.2 Computing platform

To evaluate the decomposition methods on light field (i) an 8-core CPU (Intel CoreTMi7 processor) with 12GB of RAM is used. For computations on light field dataset (ii), a cluster of 16 m3.large nodes (machines) on Amazon EC2 is instantiated. Each node has 16 cores (two Intel Xeon processors) at 7.5GB of RAM per node. The synthetic datasets are evaluated on IBM iDataPlex computing cluster which has 2304 cores in 192 Westmere nodes (12 processor cores per node) at 48GB of RAM per node.

6.1.3 Distributed tools

The RankMap framework’s sparse graph-based design is implemented using *GraphLab*, a high-level graph-parallel abstraction [5]. GraphLab enables vertex-update-based computations. We implemented RankMap’s customized partitioning using Graphlab’s *ingress* class. The proposed architectures are mapped efficiently into GraphLab API (Section 5.3). Note that the GraphLab framework is designed to accelerate distributed learning for sparse graphs and thus it is not suited to process dense data until we sparsify the data using CSSD.

The RankMap framework’s sparse matrix-based computations is implemented using Eigen library to represent data in a compressed column storage (CCS) format [35]. It uses MPI standard system to distribute the data and computation and is written in C++. We have also implemented the distributed update on the factorized data on Apache Spark [21].

6.2 Scaling of CSSD

Figure 5 shows how the runtime of CSSD scales as the number of processors increases for the VideoDict dataset. We increase the number of cores from 4 to 256 (on IBM iDataPlex cluster). The dotted line shows the ideal scale-out behavior. As can be seen, CSSD is highly parallel as it almost linearly scales with the number of processors. Thus, it can be applied to very large datasets.

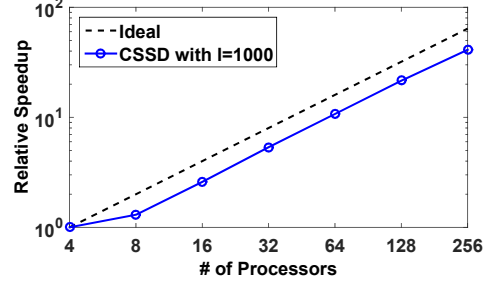


Figure 5: CSSD’s runtime scaling behavior as the number of processors increases.

6.3 Sparse approximation

To evaluate the performance of RankMap for sparse approximation, we use the *fast iterative shrinkage-thresholding algorithm (FISTA)* [11] to solve the ℓ_1 -minimization problem in Equation 2. We study the utility of RankMap for two applications of the sparse representation problem discussed in Section 2.2. The applications include, sparse representation-based classification for face recognition and image denoising.

6.3.1 Sparse representation-based classification for face recognition

To employ sparse approximation for classification, our aim is to use a collection of labeled images (training set) as our dictionary \mathbf{A} and then form a sparse representation of a test image \mathbf{y} in terms of \mathbf{A} . Upon finding a sparse coefficient vector \mathbf{x} which provides a sparse approximation of $\mathbf{y} \approx \mathbf{Ax}$, we can then determine which test signals (columns of \mathbf{A} or non zeros in \mathbf{x}) are selected to represent the test signal \mathbf{y} . Based upon the class of the selected columns, we then make a decision about which class the test signal lies in. One easy way to do this is to simply sum the absolute value of the coefficients in \mathbf{x} in a certain class and then find the class that has the maximum sum.

In Figure 6a, we provide a demonstration of sparse representation-based classification for face recognition. We show the test image of interest on top and the corresponding sparse coefficient vector obtained by solving Equation 2 with FISTA for $\lambda = 1$. We solve FISTA with the full Gram matrix $\mathbf{A}^T \mathbf{A}$ and approximate Gram provided by CSSD, where the decomposition error $\delta_D = 0.05$ ($l = 62$).

To understand the connection between the decomposition error and learning accuracy for face recognition, we solve Equation 2 using FISTA for two different regularization parameters $\lambda = \{0, 1\}$, where $\lambda = 0$ corresponds to the least-squares solution and $\lambda = 1$ produces sparse solutions. We vary the decomposition error $\delta_D = \{0.4, 0.2, 0.1, 0.05\}$ and solve FISTA for 30 different test images (after removing them from training) for each of these decompositions. For

each decomposition, we calculate the: learning accuracy by measuring the ℓ_2 -norm between the solution obtained with the full and approximate Gram (Figure 6b), the sum of coefficients in the correct class (Figure 6c), and the relative density of \mathbf{V} or the number of non-zeros in \mathbf{V} versus the number of non-zeros in \mathbf{A} (Figure 6d). In Figure 6c, we also display the minimum sum of coefficients required to correctly classify the test image. These results suggest that while learning accuracy might be relatively large for high amounts of decomposition error, correct classification is possible even for large amounts of decomposition error (i.e., correct classification occurs for all test images when $\delta_D < 0.2$).

6.3.2 Light field image denoising

We evaluate RankMap’s performance in solving the Light Field data reconstruction problem. In all the following experiments dataset Light Field (ii) is used. A light field is a multi-dimensional array of images. Each image is captured from a slightly different viewpoint. Combining the images enables creating new views and representing observer positions not present in the original array. Most currently available devices trade image resolution for the ability to capture different views of a light field. As a result, the final image resolution is reduced by orders of magnitude compared to the sensor resolution. To address this challenge, ℓ_1 -minimization (Equation 2) is employed to find a sparse representation of a light field image patch with respect to an *over-complete light field dictionary* consisting of a large number of light field image patches collected from many scenes [36].

We first apply CSSD for decomposing the dictionary corresponding to the Light Field (ii) dataset. Two different l values (240 and 1000) are used in Algorithm 1. The decomposition error δ_D is set to 0.1. We then evaluate FISTA on the decomposed data for matrix-based models. We also implement a tailored distributed MPI-based model to evaluate FISTA on the original datasets (\mathbf{A}) using regular dense matrix representations. In the following, we refer to this model as *baseline*.

Peak Signal to Noise Ratio (PSNR) is the ratio between the maximum possible power of a signal and the power of the corrupting noise. PSNR is most commonly used to measure the quality of reconstruction of noisy images and is defined as $10 \log_{10}(\frac{MAX}{\sqrt{MSE}})$ (dB). MAX is the maximum pixel value of the original image patch and MSE is the mean square reconstruction error defined as $\frac{\|y - \hat{y}\|_2^2}{m}$. In our experiments $MAX = 0.0255$. Generally, higher PSNRs indicate the better quality of reconstruction. Typical recommended PSNR values in image noise reduction application are 30 dB and higher [37, 38, 15].

Table 1 shows the total runtime of FISTA to achieve different PSNRs. In all the experiments, a batch of 10 noisy input patches is used as the input. The norm of the noise is 0.3 of the norm of the input vector (PSNR=21.14). It can be observed that by running FISTA on the decomposed data, the same PSNR is reached much faster in comparison with running FISTA on \mathbf{A} . We observe that the runtime to achieve the same PSNR is orders of magnitude faster compared to the baseline. For instance, if our desired PSNR is 30.0 dB, running FISTA on the decomposed takes 13.9s ($l=240$) and 162s ($l=1000$) while it takes 1050s for the baseline. However, as expected, the baseline (\mathbf{A}) reaches higher PSNRs in comparison with those achieved from running FISTA on the

decomposed data. For example, while the baseline’s highest achieved PSNR at convergence is 48.5 dB, it is 31.3 dB and 38.5 dB for $l = 240$ and $l = 1000$ respectively.

Table 1: FISTA runtime (s) to reach to a specific PSNR.

PSNR (db)	$l = 240$	$l = 1000$	baseline (\mathbf{A})
25	4.2	72	487
30	13.9	162	1050
35	-	356	2051
40	-	-	3171

6.4 Power method

We also evaluate our framework on power method discussed in Section 2.2. Three datasets, namely Salinas, VideoDict, and Light Field (i) have been evaluated. The matrix-based mode is used and the experiments are run on 64 cores on IBMiDataplex server. We run CSSD with various decomposition errors (δ_D) that belong to the following set: $\{0.4, 0.2, 0.1, 0.05, 0.001\}$ and run power method on each of the decomposition results. Figure 7a shows the sparsity results as we vary the error. As expected, for larger error tolerances, a higher sparsity is achieved. Figure 7b shows the impact of the decomposition error on the accuracy of the results of the power method. Here the learning error (δ_L) is defined to be the normalized accumulated error of the first 100 eigenvalues are achieved from running power method on the decomposed data versus those achieved by \mathbf{A} (baseline). By lowering the decomposition error, we can observe significant improvements in the accuracy of the power method results. Finally, Figure 7c shows the corresponding normalized runtimes to find the first 100 eigenvalues. It can be observed that significant speedups in comparison with the baseline is achieved.

6.5 Graph- vs. matrix-based models

We compare the performance of RankMap’s proposed vertex and matrix-based models for various synthetic decomposed data. The purpose of these evaluations is to determine the advantage of each of the models with respect to the structure of the data. In all the experiments, the iterative update in Equation 3 is applied on a random input vector \mathbf{y} . The experiments are done on an IBM iDataplex computing cluster. In all the figures, the runtime results for the dense matrix-based implementation (i.e., regular deployment of the decomposed matrices without using CCS format) are also provided to demonstrate the efficiency achieved by exploiting sparsity in \mathbf{V} through graph-based and sparse matrix-based models.

Figure 8a shows the performance for different (block-diagonal) \mathbf{V} ’s with fixed number of non-zeros (set to $100M$). Thus as l increases, the density-level of \mathbf{V} would decrease. Graph-based model’s performance is more consistent as l increases. However, the matrix-based model’s performance degrades for larger l ’s. This observation can also be explained due to the fact that the communication overhead of the matrix-based model is more affected by larger l ’s.

Figure 8b shows the performance for a fixed $l = 500$ on block-diagonal matrices \mathbf{V} for varying densities of \mathbf{V} . As density increases, the performance decreases in both models. However, the performance degradation in graph-based model is worse due to the overhead of representing a large

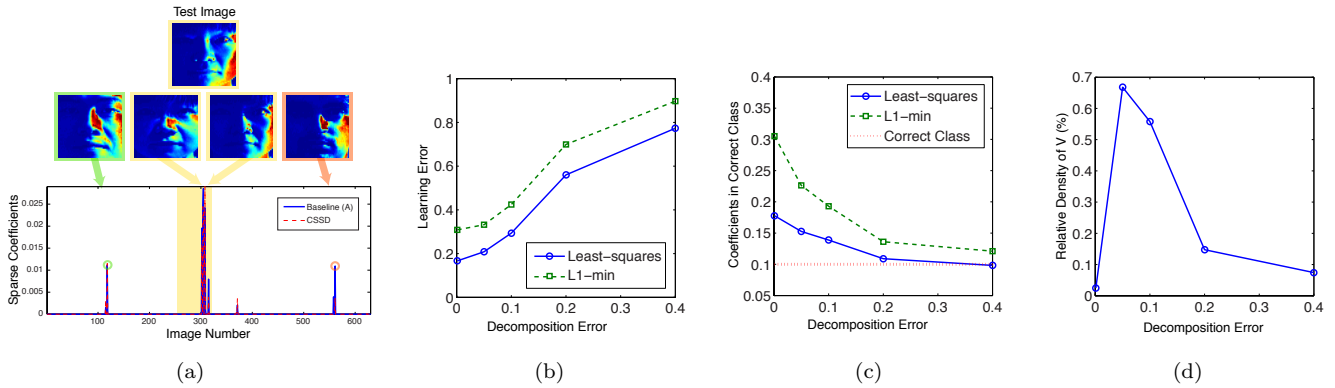


Figure 6: Sparse representation-based face recognition. (a) On top, we display a test image; on the bottom, we display the sparse solution obtained with the original Gram (blue, solid) and approximate Gram with CSSD for $\delta_D = 0.05$ (red, dash). We display four training images corresponding to non zero coefficients: large amplitude coefficients correspond to images in the correct class and smaller amplitude coefficients correspond to images in incorrect classes. The block of coefficients corresponding to images in the correct class are highlighted. For a range of decompositions (varying δ_D) we show (b) learning accuracy which measures the 2-norm between the solution obtained with the full and approximate Gram, (c) sum of coefficients in the correct class, the minimum sum of coefficients required to correctly classify the test image is also shown. and (d) relative number of non-zeros in \mathbf{V} versus the number of non-zeros in \mathbf{A} .

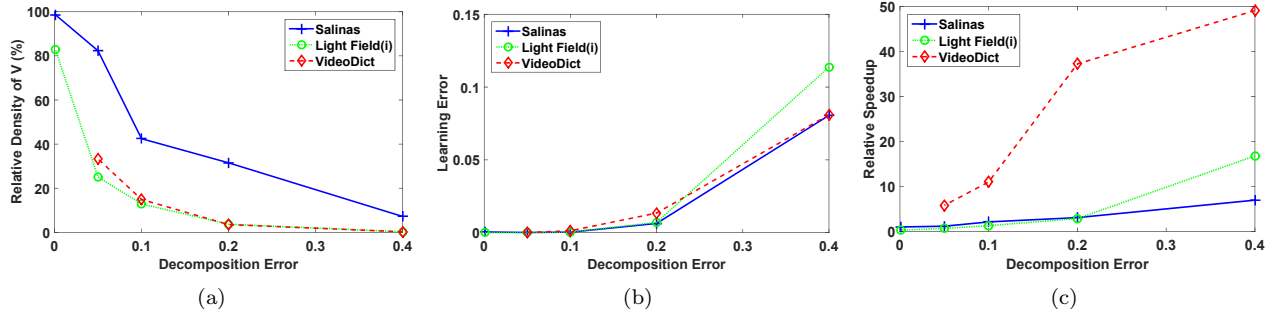


Figure 7: Power method results for three datasets: Salinas, VideoDict, and Light Field (i). Effect of varying the decomposition error (δ_D) on (a) sparsity. Reported values are the number of non-zeros in decomposition factor \mathbf{V} normalized to the number of non-zeros in \mathbf{A} , (b) the learning error (δ_L), and (c) the relative speedup of power method to find the first 100 eigenvalues. Relative values are runtime of power method using the decomposed factors derived from CSSD normalized to the corresponding runtime using \mathbf{A} .

number of edges. Lastly, Figure 8c shows the scaling performance of the models for various number of processors. When the number of processors are less than 12, the computations are done on a single node. Thus the reverse scaling behavior while increasing the number of processors from 8 to 16 is due to the high overhead of the inter-node communication cost. For comparison purposes, the scaling performance of the baseline dense $m = 1k$ by $n = 10M$ dataset (before decomposition) is provided. It can be seen that as the number of processors increases, the performance gap between different methods shrink. However, even with a large number of processors (≥ 100), the decomposed models perform up to 2 orders of magnitude better than the baseline.

These experiments provide insights on the use-case of each model. Depending on the structure of the decomposed data and the specifications of the platforms an appropriate model should be selected. A more systematic domain-specific approach for model selection is the subject of future work.

7. CONCLUSION

This paper introduces RankMap, a novel distributed framework for applying a host of iterative learning algorithms on large-scale dense and structured datasets. Our framework leverages *low-dimensional structure* in datasets in order to map a large dataset with dense dependencies into lower dimensional components with sparse representations. Both matrix-based and graph-based distributed computational models were designed to efficiently carry out iterative update algorithms on the decomposed components. We provide guidelines on the use cases of each model based upon the decomposed data structures and the underlying computing platform. An efficient partitioning of the computational flow is developed that guarantees load balancing and significantly lowers communication overhead. We evaluate the performance of RankMap on sparse recovery and power method algorithms on various datasets and demonstrate significant improvements in runtime and memory footprint.

7.1 Decomposition overhead

RankMap applies the CSSD method offline and then uses the decomposed components for efficient execution of var-

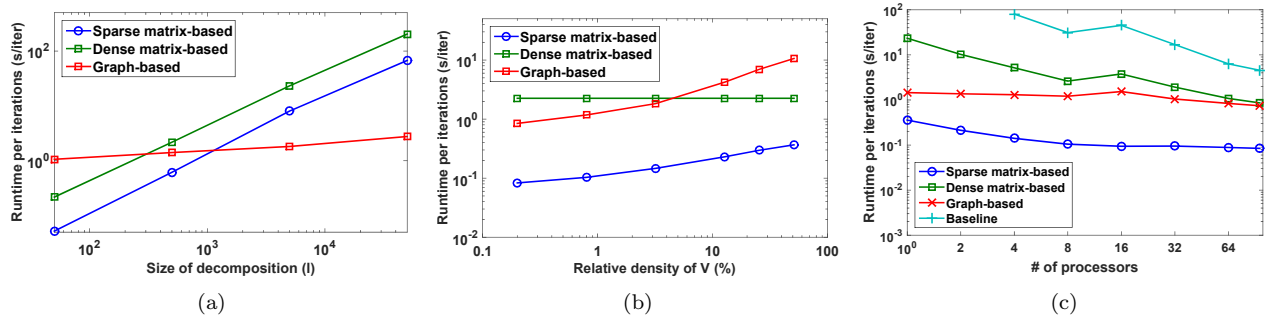


Figure 8: Results on synthetic block diagonal data: (a) runtime vs. l , (b) relative density of V , and (c) number of processors.

ious iterative update algorithms. The performance gain achieved on the subsequent computations justifies the one-time decomposition overhead. For example, we decompose Light Field dataset (ii) (Section 6) on a cluster of 4 nodes (each with 12 cores) on IBM iDataPlex. For $l = 240$, the decomposition is completed in less than 15 minutes. For 10 sample patches (each of length $18k$) the overall reconstruction time is reduced from more than 1000s to below 20s. Thus, the offline decomposition overhead can be justified once considering that there are thousands of patches in a single light field. Moreover, the same dictionary can be used to reconstruct other light field datasets.

7.2 Model selection

In Section 5, we introduced a graph-based and matrix-based computational model; thus, it is natural to ask which model to select for data processing. Both models follow the same computational flow and operate only on the non-zeros. However, due to the higher overhead of the graph-based model for storing vertices and edges, it may consume more memory. The main advantage of the graph-based model instead is in its reduced communication cost. As discussed in Section 5.3.2, when V is approximately block diagonal, the communication cost in the graph-based model is reduced. In particular, when V is completely block diagonal the communication becomes almost independent of the number of computing nodes n_c and is only proportional to $2l$. In contrast, the communication cost in the matrix-based model is always proportional to $2ln_c$. This difference may result in a better overall performance of the graph-based approach, especially for larger l and n_c values. In general, the performance of each model is highly dependent on the specifications of the available computing nodes. Our evaluations in Section 6.5 also provide insightful guidelines on the differences of the two models.

7.3 Alternative decomposition strategies

While sparse matrix factorization approaches such as SPCA and KSVD have objectives similar to CSSD, their complexity make them inapplicable to massive datasets. Our proposed decomposition instead is fast and scalable. Our CSS-based approach creates the decomposition factor D from a subset of columns of A . However, both SPCA and KSVD require costly computations to create D which requires computing the SVD of the data. Note that in addition to proposing an scalable decomposition, our framework for the first time introduces and successfully implements the idea of creating error-tunable sparse decompositions for efficient ex-

ecution of iterative learning algorithms on big and densely dependent datasets. Whilst our decomposition method is very effective, the decomposition phase in RankMap (Figure 2) can be readily replaced by other sparse decomposition approaches.

8. REFERENCES

- [1] D. C. Montgomery *et al.*, *Introduction to linear regression analysis*, 2012.
- [2] U. Nodelman *et al.*, “Expectation maximization and complex duration distributions for continuous time bayesian networks,” 2012.
- [3] G. Malewicz *et al.*, “Pregel: a system for large-scale graph processing,” *SIGMOD*, pp. 135–146, 2010.
- [4] Y. Low *et al.*, “GraphLab: A new parallel framework for machine learning,” *UAI*, pp. 340–349, 2010.
- [5] J. Gonzalez *et al.*, “Powergraph: Distributed graph-parallel computation on natural graphs,” *OSDI*, pp. 17–30, 2012.
- [6] K. Chen, “On a class of preconditioning methods for dense linear systems from boundary elements,” *SIAM*, pp. 684–698, 1998.
- [7] A. G. Gray and A. W. Moore, “N-Body problems in statistical learning,” *NIPS*, pp. 521–527, 2000.
- [8] S. S. Chen *et al.*, “Atomic decomposition by basis pursuit,” *SIAM*, pp. 33–61, 1998.
- [9] J. Wright *et al.*, “Sparse representation for computer vision and pattern recognition,” *IEEE*, pp. 1031–1044, 2010.
- [10] I. Daubechies *et al.*, “An iterative thresholding algorithm for linear inverse problems with a sparsity constraint,” *CPAA*, pp. 1413–1457, 2004.
- [11] A. Beck and M. Teboulle, “A fast iterative shrinkage-thresholding algorithm for linear inverse problems,” *SIAM JIS*, pp. 183–202, 2009.
- [12] A. E. Hoerl and R. W. Kennard, “Ridge regression: Biased estimation for nonorthogonal problems,” *Technometrics*, vol. 12, no. 1, pp. 55–67, 1970.
- [13] E. Elhamifar and R. Vidal, “Sparse subspace clustering: algorithm, theory, and applications,” *TPAMI*, pp. 2765–2781, 2013.
- [14] H. Zou, T. Hastie, and R. Tibshirani, “Sparse principal component analysis,” *JCGS*, pp. 265–286, 2006.
- [15] M. Aharon, M. Elad, and A. Bruckstein, “K-SVD: An algorithm for designing overcomplete dictionaries for sparse representation,” *TSP*, pp. 4311–4322, 2006.

- [16] M. Journée *et al.*, “Generalized power method for sparse PCA,” *JMLR*, pp. 517–553, 2010.
- [17] P. Drineas and M. Mahoney, “On the nystrom method for approximating a gram matrix for improved kernel-based learning,” *JMLR*, pp. 2153–2175, 2005.
- [18] P. Drineas, A. Frieze, R. Kannan, S. Vempala, and V. Vinay, “Clustering large graphs via the singular value decomposition,” *JML*, pp. 9–33, 2004.
- [19] C. Fowlkes *et al.*, “Spectral grouping using the nystrom method,” *TPAMI*, pp. 214–225, 2004.
- [20] J. Dean and S. Ghemawat, “MapReduce: simplified data processing on large clusters,” *CACM*, pp. 107–113, 2008.
- [21] M. Zaharia *et al.*, “Resilient distributed datasets: A fault-tolerant abstraction for in-memory cluster computing,” in *USENIX NSDI*, 2012, pp. 2–2.
- [22] A. Ghoting *et al.*, “Systemml: Declarative machine learning on mapreduce,” in *ICDE*, 2011, pp. 231–242. [Online]. Available: <http://dx.doi.org/10.1109/ICDE.2011.5767930>
- [23] G. Davis, S. Mallat, and Z. Zhang, “Adaptive time-frequency decompositions,” *Opt. Engin SPIE*, pp. 2183–2191, 1994.
- [24] A. Deshpande *et al.*, “Matrix approximation and projective clustering via volume sampling,” in *SIAM. ACM*, 2006, pp. 1117–1126.
- [25] R. Rubinstein, M. Zibulevsky, and M. Elad, “Efficient implementation of the k-svd algorithm using batch orthogonal matching pursuit,” *CS Technion*, 2008.
- [26] R. Ramamoorthi, “Analytic PCA construction for theoretical analysis of lighting variability in images of a lambertian object,” *TPAMI*, pp. 1322–1333, 2002.
- [27] K. Kanatani, “Motion segmentation by subspace separation and model selection,” *ICCV*, pp. 586–591, 2001.
- [28] R. G. Baraniuk *et al.*, “Model-based compressive sensing,” *TIT*, pp. 1982–2001, 2010.
- [29] E. L. Dyer, A. C. Sankaranarayanan, and R. G. Baraniuk, “Greedy feature selection for subspace clustering,” *JMLR*, pp. 2487–2517, 2013.
- [30] C. Cortes, M. Mohri, and A. Talwalkar, “On the impact of kernel approximation on learning accuracy,” in *AI Statistics*, 2010, pp. 113–120.
- [31] “The Light Field Archive,” lightfield.stanford.edu, 2008.
- [32] <http://www.ehu.es/ccwintco/index.php>.
- [33] Y. Hitomi, J. Gu, M. Gupta, T. Mitsunaga, and S. K. Nayar, “Video from a single coded exposure photograph using a learned over-complete dictionary,” in *ICCV. IEEE*, 2011, pp. 287–294.
- [34] A. S. Georgiades *et al.*, “From few to many: Illumination cone models for face recognition under variable lighting and pose,” *IEEE TPAMI*, pp. 643–660, 2001.
- [35] G. Guennebaud *et al.*, eigen.tuxfamily.org, 2010.
- [36] K. Marwah *et al.*, “Compressive light field photography using overcomplete dictionaries and optimized projections,” *ACM TG*, 2013.
- [37] J.-L. Starck, E. Candes, and D. Donoho, “The curvelet transform for image denoising,” *Image Processing, IEEE Transactions on*, pp. 670–684, 2002.
- [38] E. Cands, M. Wakin, and S. Boyd, “Enhancing sparsity by reweighted ℓ_1 minimization,” *Journal of Fourier Analysis and Applications*, pp. 877–905, 2008.